Cement and Concrete Research 41 (2011) 255–262

Contents lists available at ScienceDirect

Cement and Concrete Research

journal homepage: http://ees.elsevier.com/CEMCON/default.asp

A fracture mechanics approach to the crack formation in alkali-sensitive grains

H.W. Reinhardt [a,*], O. Mielich [b]

[a] Department of Construction Materials, University of Stuttgart, Pfaffenwaldring 4, D-70569 Stuttgart, Germany
[b] Materialprüfungsanstalt Universität Stuttgart, Pfaffenwaldring 4, D-70569 Stuttgart, Germany

ARTICLE INFO

Article history:
Received 2 July 2010
Accepted 17 November 2010

Keywords:
Alkali–aggregate reaction (C)
Durability (C)
Expansion (C)
Fracture toughness (C)

ABSTRACT

The cause of cracking of slow/late aggregates is supposed to be due to gel pressure in the grain. The cracking of grains is approached with the aid of fracture mechanics and the decisive parameter for crack extension is the critical stress intensity factor. Various types of rock were stored in alkaline solution. The critical stress intensity factor was determined as function of exposure time. A theoretical correlation between grain size, critical stress intensity factor, and gel pressure was established.

1. Introduction

Alkali–silica reaction (ASR) is a degradation process of concrete which has numerous aspects. One concerns the so-called slow/late aggregates which react only after several years of exposure. Another concerns the mechanism of crack formation in concrete. The literature contains and describes two fundamentally different mechanism of degradation. One mechanism claims that dissolution takes place at the surface of the aggregate grain [1] and that a gel develops at the surface of the grain which can crack the matrix around the grain due to swelling pressure. This mechanism is discussed in detail by Diamond [2]. The other theory states that internal cracks form in the grain also due to gel formation which extend into the matrix and leads finally also to cracks in concrete [3–5]. The second approach assumes that a critical expansion of the aggregate must be reached in order to start cracking. The ASR induced degradation is modeled with finite elements in [6] assuming a critical stress as failure criterion. However, here it is argued that cracks develop due to a dissolution process and that a critical crack length must exist before the grain can be split. Final splitting is caused by the swelling pressure of a gel. Whereas [3–6] assume either a limiting strain or a limiting stress as failure criterion the fracture toughness is regarded as the decisive parameter for crack extension. Fracture mechanics has been developed to describe the limit state of brittle materials under load. In fracture mechanics terms the stress field around a crack is calculated in which the stress intensity factor is the governing parameter. When the stress intensity factor reaches the critical stress intensity factor which is a characteristic parameter of the material a crack propagates. This approach will be applied to slow/late aggregates.

2. Fracture mechanics approach

According to the theory of linear-elastic fracture mechanics the stress around the tip of a sharp crack is given by a function of the stress intensity factor. The stress intensity factor depends on the loading and the geometry of the situation considered. There are several books available which list the stress intensity factors for many geometries, see for instance [7–10]. In the current study, a grain is idealized as sphere with a penny-shaped crack in the center. Fig. 1 shows the situation with R = radius of the sphere and a = radius of the crack. x, y, z are the coordinates.

In the interior of the crack, the uniform pressure p_0 is acting. If R is infinite the solution of the crack intensity factor reads for linear-elastic material [10]

$$K_I^{\infty} = \frac{2}{\pi}\cdot p_0 \cdot \sqrt{\pi \cdot a} \tag{1}$$

If the sphere has a finite radius Eq. (1) has to be corrected by the shape factor $Y(a/R)$. For $a/R \le 0.60$, the closed-form solution reads [11]

$$Y(a/R) = \frac{K_I}{K_I^{\infty}} = 1 + 1.5433\cdot\left(\frac{a}{R}\right)^3 - 2.3870\cdot\left(\frac{a}{R}\right)^5 + 2.3818\cdot\left(\frac{a}{R}\right)^6 + 3.2711\cdot\left(\frac{a}{R}\right)^7 - 6.4470\cdot\left(\frac{a}{R}\right)^8 - 0.2107\cdot\left(\frac{a}{R}\right)^9 + 0\cdot\left(\frac{a}{R}\right)^{10} \tag{2}$$

For $a/R > 0.60$ numerical methods have to be applied. Table 1 gives some numerical values of $Y(a/R)$.

* Corresponding author.
E-mail address: reinhardt@iwb.uni-stuttgart.de (H.W. Reinhardt).

0008-8846/$ – see front matter © 2010 Elsevier Ltd. All rights reserved.
doi:10.1016/j.cemconres.2010.11.008

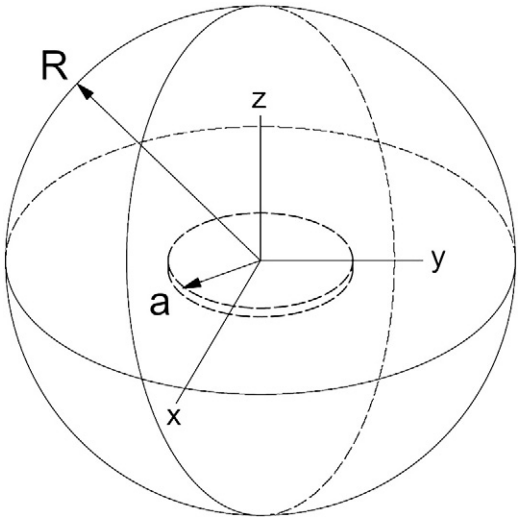

Fig. 1. Central penny-shaped crack in a sphere.

The table shows that the values start with 1 for $R=\infty$ and go up to 1.81071 for $a/R=0.9$. Crack extension occurs when the stress intensity factor reaches the critical stress intensity factor K_{Ic} which is a material property and has to be determined experimentally.

3. Determination of fracture toughness

Fracture toughness has been measured as critical stress intensity factor on circular rods with a chevron notch. The method follows the proposal of the International Society for Rock Mechanics (ISRM) [12] applying the so-called CENRBB specimens (Chevron Edge Notch Round Bar Bending). Fig. 2 shows the testing arrangement and Fig. 3 shows the middle cross-section.

A central force F is applied while the crack mouth opening displacement (CMOD) is used as the control quantity. The constant crack mouth opening displacement rate was 0.13 μm/s. The length of the specimen is denoted L, the diameter D, the chevron angle θ, the depth of the notch tip is at a_0, and the width of the notch is denoted t. Table 2 gives the dimensions of the specimen as requested by ISRM [12] and the values as chosen in the experiments.

The grain size of the rock for the aggregates is in the order of 3 mm. The specimens were drilled from large size blocks taken from the quarry or from large rounded rocks from sand pits. The critical stress intensity factor can be calculated with Eq. (3)

$$K_{Ic} = \frac{A_{min} \cdot F_{max}}{D^{1.5}} \tag{3}$$

with F_{max} the maximum force, D the diameter of the specimen, and A_{min} a geometrical factor which follows from Eq. (4)

$$A_{min} = \left[1.835 + 7.15 \cdot \frac{a_0}{D} + 9.85 \cdot \left(\frac{a_0}{D}\right)^2\right] \cdot \frac{S}{D} \tag{4}$$

with a_0 the notch-tip depth and S the span of the specimen. This calculation is valid for linear-elastic material. Since rock is not ideally elastic one has to consider a correction factor which can be calculated in a rather elaborate procedure. The procedure takes account of several loading and unloading cycles which characterize the non-linear part of the force-crack mouth opening displacement curves. Fig. 4 gives an example of such a curve.

Table 1
Numerical values of Y (a/R) [11].

a/R	0	0.2	0.4	0.5	0.6	0.7	0.8	0.9
Y (a/R)	1	1.01176	1.08516	1.15549	1.27016	1.32240	1.47210	1.81071

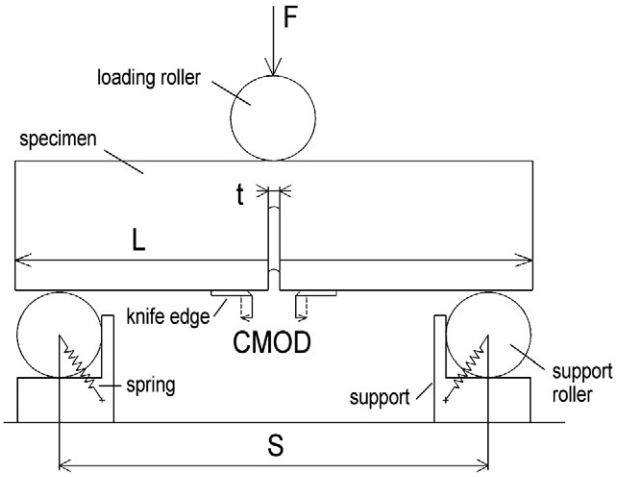

Fig. 2. Testing arrangement of fracture tests according to ISRM [12].

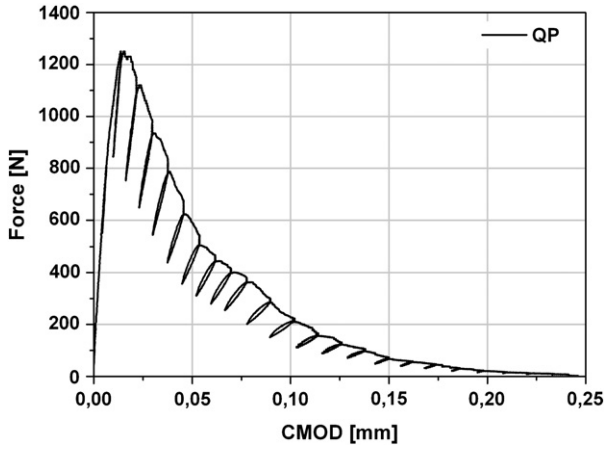

Fig. 3. Middle section CENRBB specimen according to ISRM [12].

It shows several features. First, the rock is not ideally brittle because there is a softening after the peak load has been reached. Second, the slope of the unloading curves becomes flatter with increasing number of cycles. The evaluation method of [12] uses the slope of the curve as an indicator of the non-linearity of the behavior and can deduce from that a corrected critical stress intensity factor K^c_{Ic}.

The reader is referred to reference [12] for the detailed use of the method. It should be noted that the corrected critical stress intensity factor K^c_{Ic} is always larger by 5 to 40% than the critical stress intensity factor of linear-elastic material K_{Ic}. The increase depends on the type of rock which will be shown later.

Table 2
Dimensions of the specimens according to ISRM [12] and the specimens of the actual tests.

Dimensions	Size	Tolerance	Own tests
Diameter of the specimen, D [mm]	D	> 10 · Grain size	34
Length of the specimen, L [mm]	4 · D	> 3.5 · D	120
Span of the specimen, S [mm]	3.33 · D	± 0.02 · D	113.2
Chevron notch, θ	90°	± 1.0°	90°
Notch-tip depth, a_0 [mm]	0.15 · D	± 0.01 · D	5.4
Width of the notch, t [mm]	≤0.03 · D or 1 mm[a]		1.0

[a]The larger value is decisive.

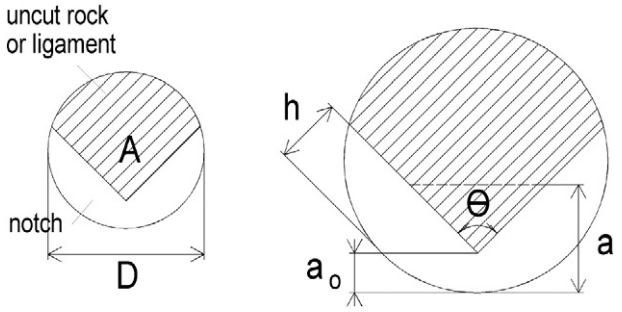

Fig. 4. Force vs. load-crack mouth opening displacement curve of quartz porphyry in the virgin state.

The CENRBB test allows also to calculate the elastic modulus by using Eq. (5) which reads

$$E = g_0 \cdot \frac{dF}{d(\mathrm{CMOD})} \cdot \frac{1}{D} \tag{5}$$

with g_0 a geometrical factor and dF/d (CMOD) the slope of the force-crack mouth opening curve. g_0 follows from

$$g_0 = 20.8 - 19.4 \cdot \frac{a_0}{D} + 142.3 \cdot \left(\frac{a_0}{D}\right)^2 \tag{6}$$

The parameters E and K^c_{Ic} will be used for further calculations.

4. Aggregates used

Six types of rocks were selected for the experiments. These were greywacke (GW) and quartz porphyry (QP) from a quarry in the middle of Germany, quartz porphyry (QP1-OR), quartzite (QZ-OR), and another quartz porphyry (QP2-OR) from sand pits of the upper Rhine valley as well as Diabase (DB) from North Bavaria. The rocks from the upper Rhine valley are rounded rocks which are deposited there after a long journey from the Alps. The alkali sensitivity of the rocks was assessed with the accelerated mortar test according to [13] which is derived from [14] and [15]. Additionally the alkali sensitivity of the rocks was assessed within a period of 540 days with the fog chamber test at 40 °C used in Germany, similar to the internationally usual concrete prism tests (RILEM AAR-3). With the mentioned tests, greywacke (GW), quartz porphyry (QP), quartzite (QZ-OR), and the quartz porphyry (QP2-OR) were found to be ASR sensitive while quartz porphyry (QP1-OR) and diabase turned out to be insensitive.

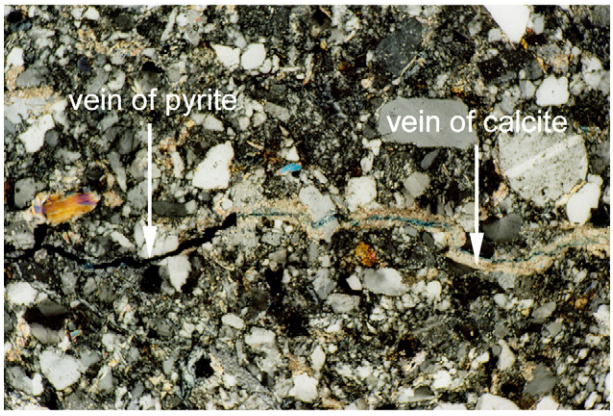

Fig. 5. Structure of greywacke with veins of pyrite and calcite under cross polarized light (image approximately 1.0 mm).

The mentioned tests which were prepared to assess the alkali sensitivity of the aggregates are described in detail by Mielich [16].

The mineral composition has been determined by X-ray diffraction. The results are given in Table 3.

The structure of the rocks has been observed under polarization microscope. The structure of greywacke is very dense. However, there are veins of pyrite and calcite visible in the interior (Fig. 5). These veins will play a major role in the degradation process.

The accessible pore volume amounted to 0.41%. Quartz porphyry belongs to the group of rhyolites. They show relatively large feldspar crystals. Fig. 6 shows the structure with veins of hematite and chlorite. The accessible pore volume amounted to 0.57%.

The quartzite consists mainly of quartz and contains some percent of mica. Fig. 7 gives an impression of the structure which shows rather large crystals. The accessible pore volume was 1.43%.

Diabase is a volcanic rock which consists for a great part of plagioclase. Fig. 8 shows the structure of diabase with clefts healed with carbonate. The accessible pore volume amounted to 0.82%.

All rocks which were subject of the experiments are very dense with low accessible porosity. However, there are inclusions which may be prone to deterioration which will be shown in the following chapter.

5. Degradation of rocks during exposure

Due to the formation of the alkali hydroxides (KOH, NaOH) during the reaction of cement and water, the concentration of OH- in the pore solution of concrete can increase up to 800–1000 mmol/l [17] if an Ordinary Portland Cement (OPC) with high alkali content (1.24 $Na_2O_{equ.}$

Table 3
Major mineral components of the rocks used.

Rock type	Mineral composition [%]						
	Quartz	Feldspar	Plagioclase	Chlorite	Carbonate	Mica	Kaolinite
Greywacke (GW)	29.0	6.8	32.9	14.1	3.2	10.8	3.2
	Quartz	Feldspar	Plagioclase	Chlorite	Carbonate	Mica	Hematite
Quartz porphyry (QP)	22.0	33.7	34.5	2.6	1.8	4.6	0.6
Quartz porphyry (QP1-OR)	17.4	22.7	41.9	9.8	1.1	6.7	0.3
	Quartz	Mica					
Quartzite (QZ-OR)	96.4	3.6					
	Quartz	Feldspar	Plagioclase	Carbonate	Hematite		
Quartz porphyry (QP2-OR)	37.9	0.9	58.2	1.9	1.1		
	Quartz	Plagioclase	Carbonate	Chlorite	Mica	Hematite	
Diabase (DB)	3.0	40.3	19.9	28.2	8.0	0.5	

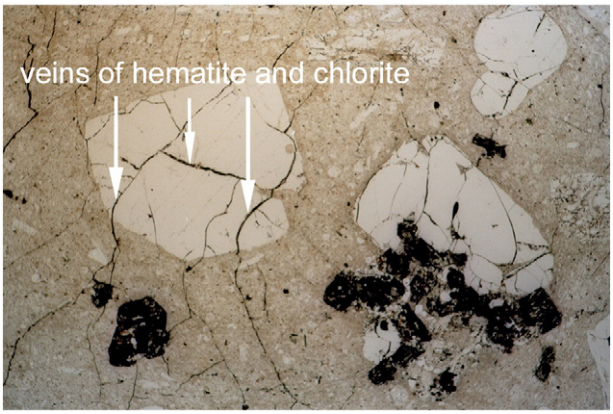

Fig. 6. Structure of quartz porphyry with veins of chlorite and hematite under planar polarized light (image approximately 6.3 mm).

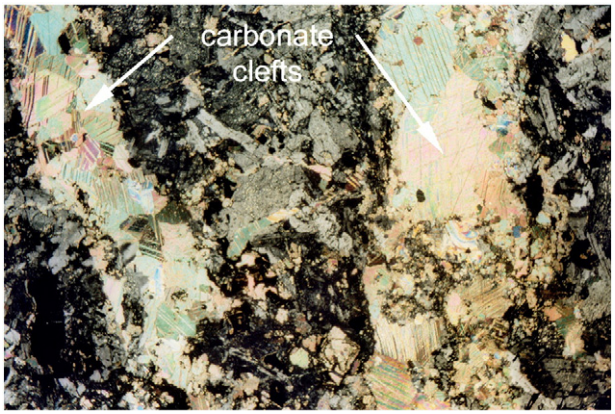

Fig. 8. Structure of diabase with carbonate clefts under planar polarized light (image approximately 6.3 mm).

by weight of cement) in concrete is used. All aggregates containing SiO_2 react in concrete with the alkali ions of the pore solution. The reaction will damage the concrete only in case of sufficient amounts of reactive SiO_2 in the aggregates as well as high alkali concentrations and high pH values in the pore solution, respectively.

To simulate the condition of a grain in concrete in respect of the concentration of OH^- only rock bars were stored in synthetic potassium hydroxide solution at the maximum concentration of OH^- (1000 mmol/l). The pH value of the synthetic hydroxide solution was 14.0. The temperature of the solution was kept at 40 °C. This is the temperature level of the fog chamber test used in Germany for testing alkali-sensitive aggregates in concrete which follows the RILEM test AAR-3 [18]. The bending tests with CENBRR samples were carried out after 0 (virgin state), 35, 70, 140, 280, and 540 days of storage in the potassium hydroxide solution.

The well-known influence of Na and thus of Ka/Na ratios in the pore solutions of concrete on the expansion behavior of concrete with alkali-sensitive aggregates in laboratory studies [19] was not taken into account because only the alkali concentration and temperature of the pore solution is important for the solubility of reactive SiO_2 and other minerals [17]. Also calcium was not considered in the synthetic pore solution because calcium in the pore solution of concrete has only an effect on the capability of swelling of gels [17,20] and not on the solubility of reactive SiO_2 and other minerals.

5.1. Degradation features

Thin sections have been made for microscopy evaluation after impregnation of the rock with a colored epoxy resin. After 560 days of storage in the alkaline solution, greywacke (GW) was a little dissolved at the surface of the rock bar. Mainly feldspar was dissolved. The dissolution zone reached to a depth of about 3 mm. The veins which were originally cemented by pyrite and calcite were completely cracked and pyrite and calcite were dissolved. Fig. 9 shows the situation.

The veins contained an alkali–silica gel of typical composition (12.7% K_2O, 29.8% CaO, 55.3% SiO_2, 2.2% Al_2O_3). The dissolved Fe ions could be observed as brown discoloring on the surface of the concrete specimens which were prepared by Mielich [16]. When the alkali content of the cement was reduced 0.89 Na_2O_{equ} by weight of cement the pH value of pore solution was reduced to 13.76 and no dissolved Fe ions and discoloring could be observed [16]. A look to the Eh-pH diagrams for mineral stability relations reveals that iron is hardly soluble at this pH [21].

The quartz porphyry (QP) had veins filled with chlorite and hematite when investigated at the beginning of the test. After 560 days of exposure, the chlorite and hematite is dissolved and the dissolution progresses into fine-grain matrix (Fig. 10).

The dissolution of the matrix increases the porosity of the rock. The quartz porphyry of the upper Rhine valley (QP1-OR) behaved totally differently. It did not show any sign of degradation.

A sample from QP2-OR (quartz porphyry of the upper Rhine valley) behaved differently again. Surface cracks appeared after 140 days of exposure. The cracks propagated and alkali–silica gel precipitated in the cracks. Fig. 11 is taken after 280 days. It shows a zone with alkali–silica gel which was possible due to the presence of Ca^+ ions of the mineral calcite.

As expected the diabase did not show signs of degradation.

The degradation of slow/late aggregates is regarded as a two steps process. The first step concerns the dissolution of the pyrite and calcite veins in the grain for which a high alkalinity in form of high pH value is necessary. The dissolution creates open cracks in the

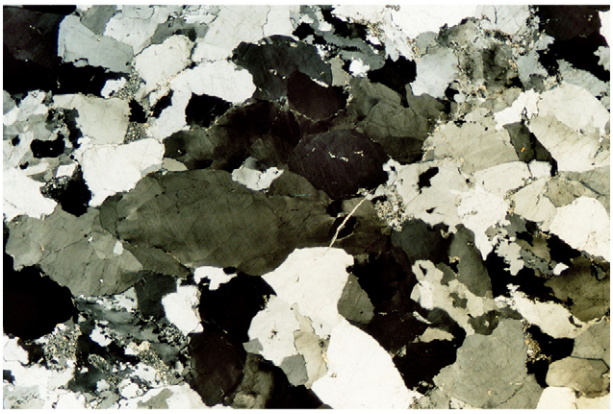

Fig. 7. Structure of quartzite under cross polarized light (image approximately 6.3 mm).

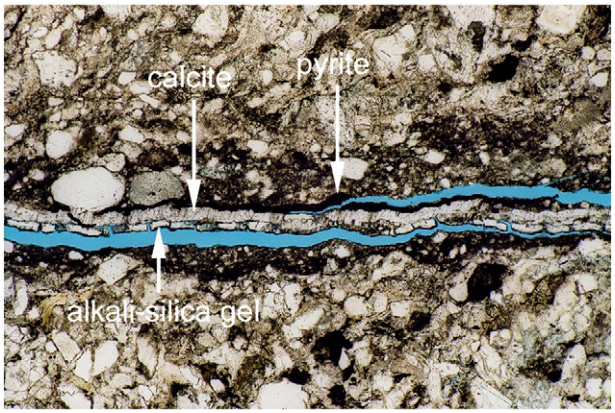

Fig. 9. Greywacke after 560 days of exposure under planar polarized light (image approximately 2.5 mm).

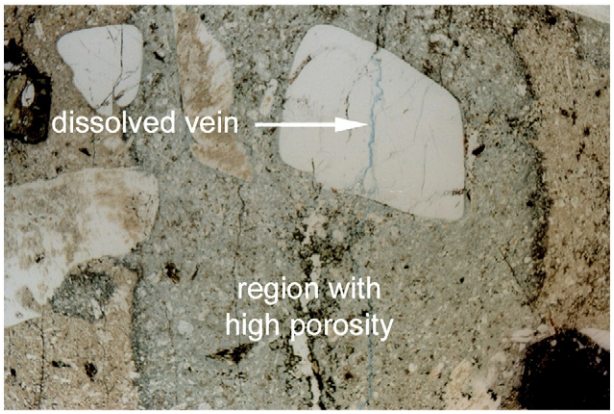

Fig. 10. Quartz porphyry after 560 days of exposure under planar polarized light (image approximately 6.3 mm).

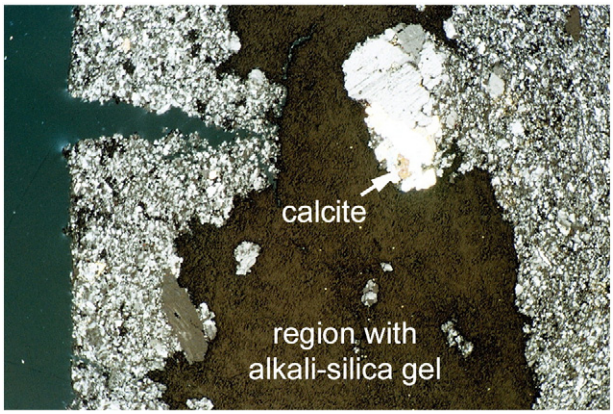

Fig. 12. Quartz porphyry of the upper Rhine valley QP2-OR after 280 days of exposure under cross polarized light (image approximately 2.5 mm).

aggregates. The second step concerns the formation of an alkali–silica gel which precipitates in the cracks. The gel swells and forces the crack to open as soon as the pressure is high enough and the critical stress intensity factor is reached. Both processes occur simultaneously and cannot be separated at the time being.

5.2. Effect of exposure on mechanical properties

When the sensitive rock is exposed to an alkaline solution the mechanical performance declines. This can be observed from Fig. 12 where the force vs. crack mouth opening displacement curves for quartz porphyry at the beginning and after 35, 70, 140, 280, and 560 days of exposure to alkaline solution are plotted.

The plot shows that the maximum force decreases and that the softening branch gets flatter with increasing exposure time. Since the maximum force determines the critical stress intensity factor proportionally it will decline accordingly (see Eq. (3)). The inclination of the linear part of the initial loading branch decreases as well with increasing exposure time. Since this determines the elastic modulus (see Eq. (5)) it will decrease as well. The softening branch is responsible for the difference between K_{Ic} and K^c_{Ic}. As will be shown in the subsequent graphs the difference between the two values of the critical stress intensity factors does not increase with increasing exposure time.

Similar curves as Fig. 12 have been evaluated with Eq. (3) for the determination of the critical stress intensity factor K_{Ic} after the intervals of exposure as stated above. The loading cycles have been also evaluated according to [12] which resulted in the adjusted critical stress intensity factor K^c_{Ic} which is always greater than K_{Ic}. Young's modulus has been calculated using Eq. (5). The mean results and the scatter band of six samples are shown in the following graphs.

Fig. 13 presents the results of greywacke. It can be seen that all three quantities vary as function of time.

The elastic modulus and K_{Ic} are almost constant during the first 140 days of exposure. After that period of time, the values decrease. The elastic modulus decreases from about 75 to 40 GPa while the K_{Ic} value decreases from 2.5 to 1.7 MN/m$^{1.5}$. The adjusted K^c_{Ic} follows an almost linear decrease from 3.3 to 2.1 MN/m$^{1.5}$ during the 560-day exposure time.

Quartz porphyry (QP) shows a different development in Fig. 14. The values of all three quantities are almost constant during the first 70 days.

After that time, a drop occurs. The elastic modulus drops from 75 to 25 GPa, whereas the critical stress intensity factor K_{Ic} falls from 2.3 to 1.1 MN/m$^{1.5}$and K^c_{Ic} goes down from 2.9 to 1.5 MN/m$^{1.5}$.

Fig. 15 shows the results of quartz porphyry (QP1-OR) from the upper Rhine valley. It can be seen that the three quantities show a small increase during the first 280 days. The exposure was not continued after that time.

Another sample of quartz porphyry (QP2-OR) was investigated and the results are plotted in Fig. 16.

The plot shows that the behavior is much different from QP1-OR. A decay of the elastic modulus and the critical stress intensity factors K_{Ic} and K^c_{Ic} can be observed in contrast to the results of QP1-OR. The results of Figs. 15 and 16 document that the variability of properties of the rocks of the upper Rhine valley is very large.

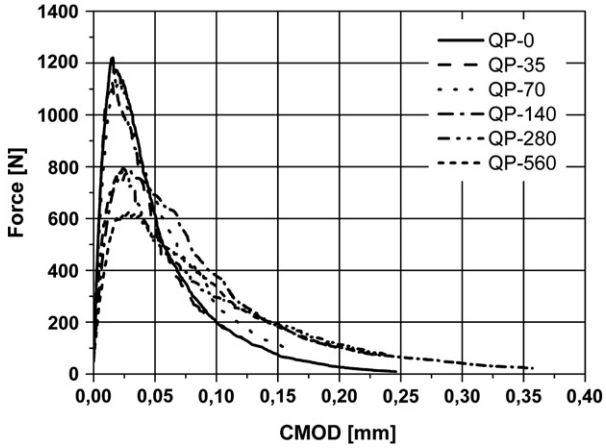

Fig. 11. Force vs. crack mouth opening displacement curves for quartz porphyry at the beginning and after 35, 70, 140, 280, and 560 days of exposure to alkaline solution.

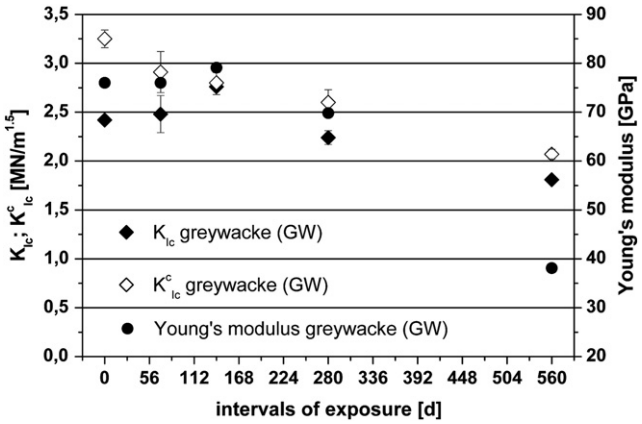

Fig. 13. Critical stress intensity factors and Young's modulus of greywacke as function of exposure time.

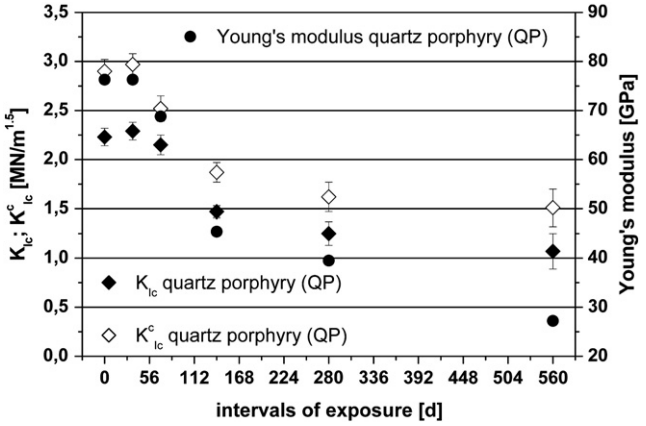

Fig. 14. Critical stress intensity factors and Young's modulus of quartz porphyry (QP) as function of exposure time.

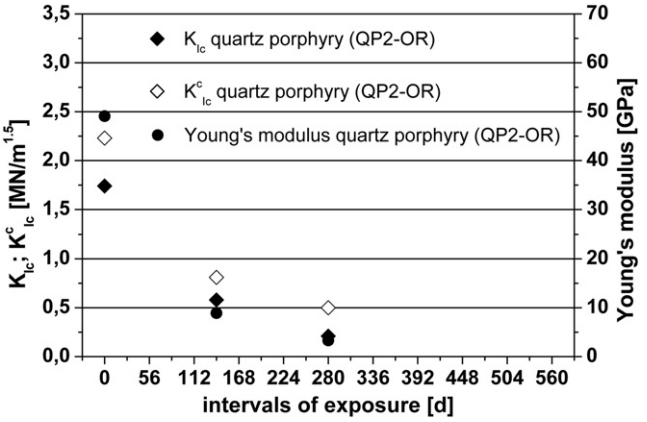

Fig. 16. Critical stress intensity factors and Young's modulus of quartz porphyry (QP2-OR) as function of exposure time.

Fig. 17 depicts the results of quartzite (QZ-OR) up to an exposure time of 280 days. The elastic modulus starts at 26 GPa and drops to 5 GPa while the K_{Ic} values decease from 1.2 to 0.6 MN/m$^{1.5}$ and the values drop from 1.5 to 0.9 MN/m$^{1.5}$.

The results of diabase (DB) are shown in Fig. 18. Although the material is known to be not sensitive to alkali–silica reaction it shows some slight influence of the exposure on the critical stress intensity factors.

Summarizing the experimental results of the exposure experiments it can be noted that most of the tested rocks deteriorate as function of time. The measured values of the critical stress intensity factor will be used in the next chapter to predict the cracking behavior of slow/late rocks in alkaline environment.

6. Discussion on internal gel pressure and crack length

The mechanism of aggregate grain splitting is assumed to be the following. Alkali ions from the concrete pore solution diffuse into the grain. They react in the interior of the grain with silicon, calcium, and aluminum ions and form an alkali–silica gel. This can happen in existing cracks or flaws or in veins which dissolve due to the pore solution. The gel expands due to the absorption of water and exerts a pressure on the flaw boundaries inside the grain. Whether this situation will lead to a splitting failure of the grain depends on the gel pressure on one side and on the crack length and the critical stress intensity factor of the rock on the other side. As soon as the critical stress intensity factor is reached the grain will split.

In order to describe the interdependence of crack length, Eq. (1) together with Table 1 has been numerically evaluated for several grain sizes. The relation reads

$$K_I(a;R;p_c) = \frac{2}{\pi}\cdot p_c\cdot\sqrt{\pi\cdot a}\cdot Y\left(\frac{a}{R}\right) \tag{7}$$

with a = crack length, R = radius of the grain which is idealized as sphere, p_c = maximum gel pressure. The gel pressure has not been investigated in this study but is taken from the literature. The literature distinguishes between those investigations of gel pressures due to ASR which were gained on mortar specimens [22–24] and those which were received from synthetic alkali gels and alkali–silica solutions [20,25]. For our investigations, only those results are relevant which were obtained from alkali gels and alkali–silica solutions. The synthetic gels of [25] reached pressures of 11 MPa. Mansfeld [20] has measured gel pressures in synthetically produced alkali gels and found values between 7.5 and 16 MPa. A maximum pressure of 20 MPa is reported in [26,27]. Additionally, a pressure of 30 MPa has been taken as upper limit. The deliberations in [24] which are based on a two-phase model with complete restraint of the expanding gel lead to pressures of 361 MPa which seems unrealistic in a real concrete. So, this pressure value is not considered further.

The results of the evaluation of Eq. (7) are plotted as function of a/R in Fig. 19 for a grain size of 8 mm, in Fig. 20 for a grain size of 18 mm and in Fig. 21 for a grain size of 32 mm.

In order to know whether splitting occurs one has to determine the intersect of a horizontal line at the relevant position of $K_I = K^c_{Ic}$.

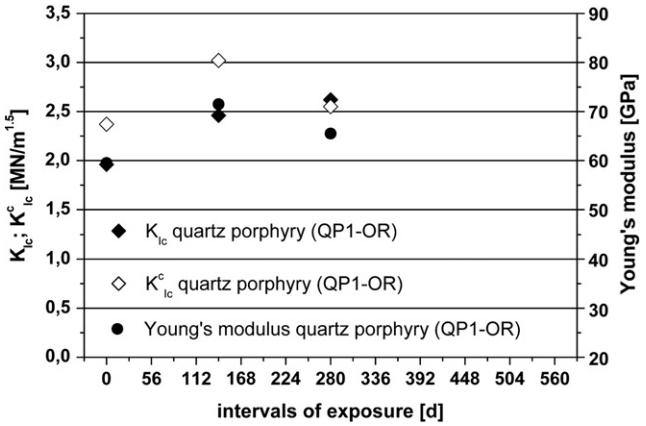

Fig. 15. Critical stress intensity factors and Young's modulus of quartz porphyry (QP1-OR) as function of exposure time.

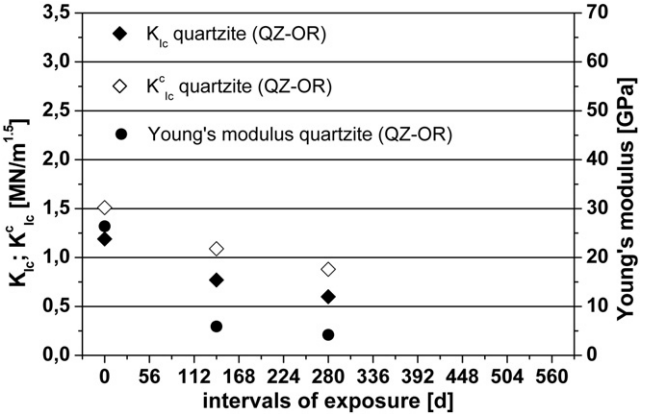

Fig. 17. Critical stress intensity factors and Young's modulus of quartzite (QZ-OR) as function of exposure time.

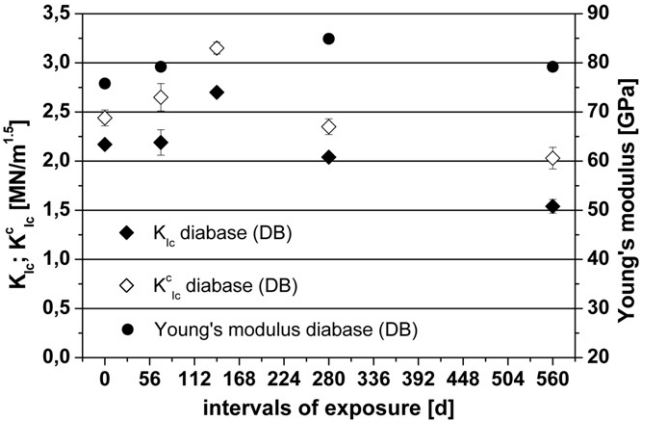

Fig. 18. Critical stress intensity factors and Young's modulus of diabase (DB) as function of exposure time.

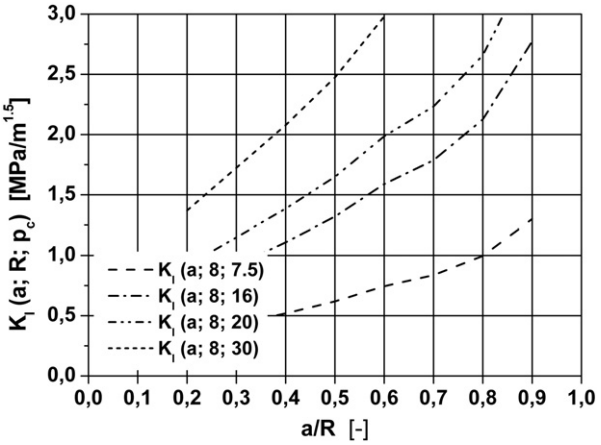

Fig. 20. Stress intensity factor as function of a/R for 16 mm grain size and gel pressures of 7.5, 16, 20, and 30 MPa.

For instance, greywacke shows a K^c_{Ic} of 2.07 MN/m$^{1.5}$ at 560 days. This means that splitting of a 16 mm grain would occur at a gel pressure of 16 MPa and a crack length of $0.75 \times 16 = 12$ mm. The theoretical prediction of crack length vs. gel pressure shall be discussed in the following, especially the question seems to be relevant whether the crack lengths which are necessary for crack propagation have been observed. Greywacke and quartz porphyry will be considered because these two rocks show large cracks and they are most suited for the application of fracture mechanics principles.

If one assumes for greywacke a gel pressure of 16–30 MPa and a grain of 16 mm diameter and considers the appropriate critical stress intensity factor of 2.60 MN/m$^{1.5}$ the penny-shaped crack should have a diameter of 14.0–8.4 mm. Such large defects have been observed due to the dissolution of pyrite veins. Also calcite veins and earlier cracks which are healed by calcite are such defects. Also the texture of layers in a grain represents a large defect. This would mean that not only crushed greywacke may be prone to ASR but also rounded greywacke grains as has been reported by Stark et al. [28].

The critical stress intensity factor for quartz porphyry was assumed to 1.72 MN/m$^{1.5}$. This would mean that a grain of 16 mm diameter would need crack length of 10.7 and 4.8 mm depending on the gel pressure of 16 and 30 MPa. The defects of this size are veins which were originally healed by chlorite and hematite. These veins are dissolved in alkaline environment and form the necessary starter cracks. Besides these defects there are micro clefts which originated from the cooling process of the molten rock.

Whether cracking will occur depends on the alkali hydroxides in the pore solution, which react with the reactive SiO_2 and the availability of calcium because these components are necessary for the formation of alkali–silica gel. When the gel forms and precipitates in the cracks the gel expands due to absorption of water. The dissolution of minerals and the formation of a gel depend on a high pH. When all prerequisites are met cracking of the grain will occur.

It can be concluded that the fracture mechanics approach is very valuable to explain the cracking of slow/late aggregates in alkaline environment. Further research will address the correlation between aggregate cracking and ASR of concrete.

7. Conclusions

Theoretical and experimental investigations have brought up the following results:

a) Linear-elastic fracture mechanics principles have been applied to aggregate grains, i.e., the critical stress intensity factor is regarded as decisive parameter which governs cracking of slow/late aggregates.
b) The critical stress intensity factor of rocks decreases with the time of exposure in alkaline environment.
c) Greywacke and quartz porphyry which were taken from a quarry showed strong degradation in alkaline solution.

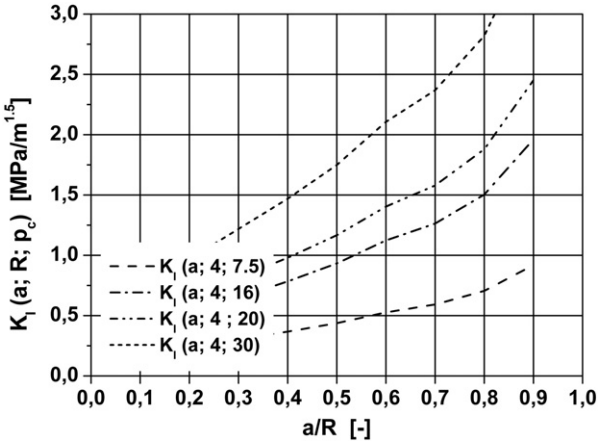

Fig. 19. Stress intensity factor as function of a/R for 8 mm grain size and gel pressures of 7.5, 16, 20, and 30 MPa.

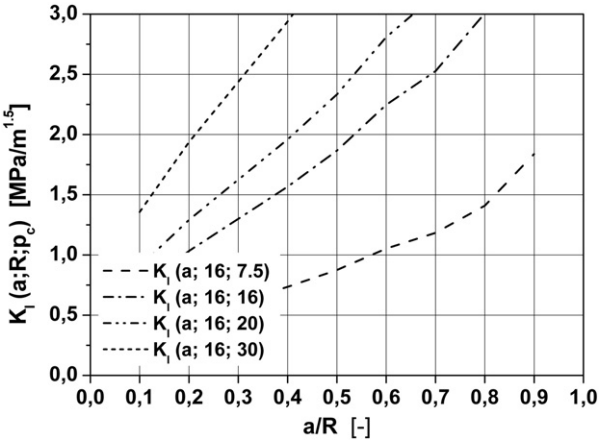

Fig. 21. Stress intensity factor as function of a/R for 32 mm grain size and gel pressures of 7.5, 16, 20, and 30 MPa.

d) Quartz porphyry from sand pits of the upper Rhine valley behaved very differently. One rock degraded considerably while another did not. The differences of deposited rocks can be very large.
e) A quartzite rock from the upper Rhine valley degraded also.
f) The degradation is due to the dissolution of chlorite, hematite, pyrite, and calcite filled veins.
g) The emptied veins form starter cracks.
h) With sufficient supply of soluble silica and calcium a alkali–silica gel forms and precipitates in the cracks. The gel expands due to absorption of water and generates a splitting pressure.
i) A correlation between the cracking of rocks, the size of the aggregate grains, and the gel pressure was established.
j) Further research is necessary to establish a correlation between the fracture of aggregate grains and ASR of concrete.

Acknowledgement

The authors acknowledge the financial support from the German Research Foundation (DFG) gratefully.

References

[1] L.S. Dent Glasser, Osmotic pressure and the swelling of gels, Cement and Concrete Research 9 (No. 4) (1979) 515–517.
[2] S. Diamond, A review of alkali–silica reaction and expansion mechanisms—2. Reactive aggregates, Cement and Concrete Research 6 (No. 4) (1976) 549–560.
[3] S. Sprung, H.M. Sylla, Course of the alkali/silica reaction in concrete with different types of aggregate, ZKG International 51 (No. 6) (1998) 334–346.
[4] M. Ben Haha, E. Gallucci, A. Guidoum, K.L. Scrivener, Relation of expansion due to alkali silica reaction to the degree of reaction measured by SEM image analysis, Cement and Concrete Research 37 (No. 8) (2007) 1206–1214.
[5] E. Garcia-Diaz, J. Riche, D. Bulteel, C. Vernet, Mechanism of damage for the alkali–silica reaction, Cement and Concrete Research 36 (No. 2) (2006) 395–400.
[6] C.F. Dunant, K.L. Scrivener, Micro-mechanical modelling of alkali–silica-reaction-induced degradation using the AMIE framework, Cement and Concrete Research 40 (No. 4) (2010) 517–525.
[7] H. Tada, P. Paris, G. Irwin, The stress analysis of cracks handbook, Del. Research Corp, St. Louis, 1985.
[8] Problems of fracture mechanics and fatigue—a solution guide, in: E.E. Gdoutos, C. A. Rodopoulos, J.R. Yates (Eds.), Kluwer Academic Publishers, Netherlands, 2003, p. 618.
[9] Y. Murakami, Stress intensity factors handbook, Pergamon Press, New York, 1987.
[10] H.G. Hahn, Fracture mechanics (in German), B.G. Teubner, Stuttgart, 1976.
[11] K.N. Srivastava, J.P. Dwivedi, The effect of a penny-shaped crack on the distribution of stress in an elastic sphere, International Journal of Engineering Science 9 (1971) 399–420.
[12] F. Ouchterlony, Suggested methods for determining the fracture toughness of rock, International Journal of Rock Mechanics and Mining Sciences and Geomechanics Abstracts 25 (1988) 71–96.
[13] L. Franke, S. Witt, Accelerated test for alkali reaction: application of an internationally recognized quick test to German conditions, Concrete Plant + Precast Technology 70 (No. 5) (2004) 14–21.
[14] R.E. Oberholster, G. Davies, An accelerated method for testing the potential alkali reactivity of siliceous aggregates, Cement and Concrete Research 16 (No. 2) (1986) 181–189.
[15] RILEM Recommended Test Method AAR-2, Detection of Potential Alkali-Reactivity of Aggregates – The Ultra accelerated Mortar-bar Test. Materials and Structures 33 (2000), No. 229, 283-289.
[16] O. Mielich, Contribution to the damage mechanisms in concrete with slow/late aggregates (in German), DAfStb Bulletin No. 583, Berlin, 2010.
[17] J. Stark, E. Freyburg, K. Seyfarth, C. Giebson, D. Erfurt, 70 years of ASR with no end in sight? (Part 1), ZKG International, No. 4, 2010, pp. 86–95.
[18] RILEM Recommended Test Method AAR-3, Detection of potential alkali-reactivity of aggregates—method for aggregate combinations using concrete prisms, Materials and Structures 33 (No. 229) (2000) 290–293.
[19] A. Leemann, B. Lothenbach, The influence of potassium-sodium ratio in cement on concrete expansion due to alkali–aggregate reaction, Cement and Concrete Research 38 (2008) 1162–1168.
[20] Mansfeld, T., Swelling behavior of alkali–silica gels with consideration of their structure and composition (in German), PhD thesis, Bauhaus-Universität Weimar, 2008.
[21] R.M. Garrels, C.L. Christ, Solutions, minerals and equilibria, Jones and Bartlett Publishers, Boston, 1965, p. 450.
[22] A. Binal, A new experimental method and device for measuring alkali–silica gel pressure in mortar, Proceedings of the 12th ICAAR, Beijing, China, 2004, pp. 266–271.
[23] A. Binal, The determination of gel swelling pressure of reactive aggregates by ASGPM device and a new reactive-innocuous aggregate decision chart, Construction and Building Materials 22 (2008) 1–13.
[24] M. Kawamura, K. Iwahori, Some theoretical considerations on expansive pressure of ASR Gel, Proceedings of the 12th ICAAR, vol. I, 2004, International Academic Publishers, Beijing, China, pp. 135–142.
[25] L.J. Struble, S. Diamond, Swelling properties of synthetic alkali silica gels, Journal of the American Ceramic Society 64 (No. 11) (1981) 652–655.
[26] German Association of Structural Concrete (DAfStb), Recommendations for damage diagnosis and repair (in German), Beton 9 (2003) 438–443.
[27] J. Stark, B. Wicht, Durability of concrete (in German), Birkhäuser, Basel, 2001, 340 pp.
[28] J. Stark, E. Freyburg, K. Seyfarth, C. Giebson, D. Erfurt, Assessment of the alkali reactivity of aggregates (in German), Beton- und Stahlbetonbau 106 (No. 8) (2007) 500–510.